

Pulse-to-pulse intensity modulation and drifting subpulses in recycled pulsars

R. T. Edwards¹ and B. W. Stappers^{2,1}

¹ Astronomical Institute “Anton Pannekoek”, University of Amsterdam, Kruislaan 403, 1098 SJ Amsterdam, The Netherlands

² Stichting ASTRON, Postbus 2, 7990 AA Dwingeloo, The Netherlands

the date of receipt and acceptance should be inserted later

Abstract. We report the detection of pulse-to-pulse periodic intensity modulations, in observations of recycled pulsars. Even though the detection of individual pulses was generally not possible due to their low flux density and short duration, through the accumulation of statistics over sequences of 10^5 – 10^6 pulses we were able to determine the presence and properties of the pulse-to-pulse intensity variations of six pulsars. In most cases we found that the modulation included a weak, broadly quasi-periodic component. For two pulsars the sensitivity was high enough to ascertain that the modulation phase apparently varies systematically across the profile, indicating that the modulation appears as drifting subpulses. We detected brighter than average individual pulses in several pulsars, with energies up to 2–7 times higher than the mean, similar to results from normal pulsars. We were sensitive to giant pulses of a rate of occurrence equal to (and in many instances much lower than) that of PSR B1937+21 at 1400 MHz (~ 30 times lower than at 430 MHz), but none were detected, indicating that the phenomenon is rare in recycled pulsars.

Key words. pulsars: general

1. Introduction

Pulsar science is perhaps unusual in astronomy, in that progress in the theoretical understanding of the emission mechanism is not limited by a lack of data, but rather by an overabundance of complex observable phenomena. Pulsar signals are seen to vary on every observable timescale from nanoseconds (e.g. Hankins et al. 2003) to decades (e.g. Weisberg & Taylor 2002), with variations associated with such phenomena as microstructure, subpulses, periodic/drifting subpulses, giant pulses, pulse nulling, mode changing, interstellar scintillation and geodetic spin precession. All of these phenomena have been important in shaping ideas concerning the radio pulsar emission process, however to date a complete explanation of radio pulsar emission remains elusive.

This discovery of PSR B1937+21 (Backer et al. 1982) posed further challenges due to its very short spin period of 1.56 ms. As more “millisecond pulsars” (MSPs) were discovered, the rapid spin and low inferred surface magnetic field strength grew to be understood as the end product of accretion from a binary companion, “recycling” pulsars that had earlier evolved into radio silence (e.g. Phinney & Kulkarni 1994). However, the question of how the radio emission mechanism is related to that of ordinary pulsars remained open. With a difference of 2–3 orders of magnitude in rotation period and

3–4 orders of magnitude in magnetic field strength, a common emission mechanism might not be expected, yet a good argument can be made for this through the comparison of (polarimetric) average pulse profile morphologies and their frequency dependence (Kramer & Xilouris 2000 and references therein).

As noted above, the true pulsar signal varies on all timescales and much has been learned about “ordinary” pulsars from studying aspects of the signal other than the basic average profile. This has not been the case with MSPs because their typically lower flux densities and shorter pulses make the detection of individual pulses difficult. An exception has been the study of so-called “giant” pulses, in PSR B1937+21 (Wolszczan et al. 1984; Backer 1995; Cognard et al. 1996; Kinkhabwala & Thorsett 2000; Vivekanand 2002; Popov & Stappers 2003), and PSR B1821–24 (Romani & Johnston 2001). Studies of the properties of pulses of normal intensity have thus far been limited to three pulsars. Sallmen & Backer (1995) used the 305-m Arecibo dish to obtain sensitivity to individual pulses of PSR B1534+12 of average and above-average energy and found that their distribution in energy was similar to that of some ordinary pulsars. On the basis of the detection of pulses of above-average intensity, both Jenet et al. (1998) and Vivekanand et al. (1998) found that the properties of the brightest known MSP, PSR J0437–4715, were similar to those of ordinary pulsars, although to good significance neither nulling nor the presence of preferred timescales within individual pulses (e.g. microstruc-

ture, subpulses) was detected. Both studies report the detection of quasi-periodic pulse-to-pulse intensity modulations with a period of ~ 4 pulses, and Vivekanand et al. (1998) report (we believe potentially erroneously; see Sect. 4) that the modulation is not associated with drifting subpulses, as it often is in ordinary pulsars. Finally, Jenet et al. (2001) used data with an average single-pulse signal-to-noise (S/N) ratio less than one to show that on a statistical basis and with the exception of giant pulses, the emission of PSR B1937+21 is extremely stable, showing to high significance a complete lack of pulse-to-pulse variations and no difference between the shape of individual pulses and that of the average profile.

As shown by Jenet et al. (2001), poor single-pulse S/N does not eliminate the possibility of obtaining useful information regarding single pulses. The average profile can of course be measured in such cases, but there is no reason why collection of statistics cannot be extended beyond the first moment to include higher-order moments and correlations. Of primary interest are the second moment¹ (giving access to the modulation index), and the second order correlations. A variety of useful correlation statistics can be derived; Jenet et al. (2001) integrated the single-pulse autocorrelation function (ACF) to show that every pulse appeared to be identical to the average profile. We extend this approach here to include the Longitude-Resolved Fluctuation Spectrum (LRFS; Backer 1970), the Two-Dimensional Fluctuation Spectrum (2DFS; Edwards & Stappers 2002) and the Longitude-Resolved Cross-Correlation Function (LRCCF; Popov 1986). Applying these techniques to archival observations made at the Westerbork Synthesis Radio Telescope (WSRT), we have detected and characterised pulse modulation behaviour in several recycled pulsars.

2. Observations and Methods of Analysis

2.1. Observations

The data used in this project were selected from archival data taken at WSRT. For many pulsars numerous observations were available, allowing us to take advantage of fortuitous scintillation conditions for substantial enhancements in sensitivity. For all observations, dual linear polarization signals from fourteen 25-m dishes were added using previously determined phase and gain factors and the resultant signal was digitally processed by the PuMa pulsar backend to form a two-dimensional array of total power samples, as a function of time and radio frequency; for details see Voûte et al. (2002). In offline processing, frequency channels containing periodic interference were flagged and a de-dispersed time series was produced by combining remaining channels, aligned using previously published dispersion measures. In Table 1 we list parameters of the observations used, including the date of observation as a Modified Julian Day (MJD), the observation duration (T_{obs}) in seconds, the centre frequency (ν) and total bandwidth ($\Delta\nu$) in megahertz, the number of frequency channels used, the resultant dispersion

¹ Since they worked from voltage samples instead of intensity samples, Jenet et al. (2001) referred to this as the fourth moment.

smearing (τ_{smear} , near the center frequency) and output sample interval (τ_{samp}) in microseconds, and the number of pulses recorded. The rightmost four columns refer to the sensitivity, see Sect. 3.1.

2.2. Production of a Longitude/Time-dependent Array

For many techniques of single pulse analysis including those used in this work, the data need to be treated as a sequence of sampled pulses, with a consistent sampling lattice within each pulse. The simplest approach to producing a such two-dimensional (i.e. longitude- and time-resolved) representation of the pulse sequence is to bin each sample according to its pulse phase, as calculated using an ephemeris (for which purpose we used the TEMPO software package²). When the time resolution is close to the interval corresponding to the desired longitude resolution, a problem arises with this method. In the simplest case, where the longitude bin width is chosen to correspond to one sample interval (at some point during the observation), each pulse as it appears in the binned sequence is effectively shifted by an amount corresponding to the offset between each sample and the bin centers. This offset advances (modulo one bin) by a constant amount each pulse due to the fact that the apparent pulse period does not (in general) equal an integer number of sample intervals. The pulse shape distortion (longitude shift) is thus periodic from pulse to pulse, and gives rise to a sequence of harmonics in the LRFS. This problem was encountered by Vivekanand et al. (1998) in their analysis of data from PSR J0437–1715, but no attempt was made to remove it.

In this work we avoided the effect by compensating for the shift in each pulse using a frequency-domain time shift. Formally, we may view the time series as a sampled signal that represents the source intensity signal, convolved with a function representing the applied integration. By using a sequence of samples that is offset from the required set of bin centers (longitude samples) by some fraction of a sample $\epsilon \in [-0.5, 0.5]$, and assigning those samples to the nearest bin, we arrive at a version of the pulse signal that is apparently longitude-shifted by ϵ samples. This can be simply corrected by convolution with an offset sinc function, which by virtue of Fast Fourier Transform algorithms is efficiently performed by multiplying the Discrete Fourier Transform (DFT) of the pulse by $\Delta(\nu_1) = \exp(2\pi i \epsilon \nu_1)$ and taking the inverse DFT³. If this correction is made to each pulse, the artifact is removed completely from the signal and all fluctuation statistics can generally be interpreted correctly.

In some circumstances, extension of the approach to effect a change in sampling interval (by dropping coefficients

² <http://pulsar.princeton.edu/tempo/>

³ Since this performs a cyclical convolution, it is necessary to discard some samples from the ends of the sequence. This is most noticeable in the presence of strong interference, when the apparent step between the last sample and the first can cause ringing at the Nyquist frequency when the sampling lattice is offset by this process. We found that discarding 32 samples from each end of the result was sufficient to avoid this effect.

Table 1. Observation parameters and sensitivity

Name (PSR)	Date (MJD)	T_{obs} (s)	ν (MHz)	$\Delta\nu$ (MHz)	N_{chan}	τ_{smear} (μs)	τ_{samp} (μs)	N_{pulses} (10^3)	σ_g	σ_m	σ_c	E_{min} ($< E >$)
J0034–0534	52216.1	1800	328	10	512	63.2	102.4	775	2.0	1.7	0.11	20
J0218+4232	52462.4	1800	328	10	1024	140.7	102.4	959	3.6	3.0	0.19	26
J0613–0200	52190.1	9000	1380	80	512	19.1	51.2	2914	3.1	2.6	0.16	19
J1012+5307	52145.7	1800	840	80	512	19.7	102.4	342	0.37	0.31	0.019	3.3
J1022+1001	52392.8	1800	1380	80	512	4.5	51.2	342	0.2	0.17	0.011	0.78
	52004.8	7200	328	10	512	47.0	102.4	433	0.29	0.24	0.015	1.5
	52004.6	7200	840	80	64	22.4	51.2	433	0.55	0.47	0.029	2.2
J1518+4904	52086.6	3600	1380	80	512	5.1	102.4	433	0.21	0.17	0.011	0.62
	52101.7	3600	1390	60	384	5.6	204.8	85	0.096	0.081	0.0057 ²	0.65
	52242.5	1800	1380	80	512	30.8	102.4	368	1.0	0.85	0.053	12
J1643–1224	52242.5	1800	1380	80	512	30.8	102.4	368	1.0	0.85	0.053	12
J1713+0747	52544.7	7200	840	80	512	35.0	51.2	1558	0.54	0.46	0.028	8.7
	52515.7	1800	1190	80	512	12.3	51.2	376	0.12	0.10	0.0064	1.8
	52537.7	3600	1700	40	256	4.2	51.2	770	0.11	0.092	0.0058	2.1
J1918–0642	52572.5	3600	2240	80	512	1.8	51.2	770	0.27	0.23	0.014	5.2
	52560.8	1800	1380	80	512	13.1	102.4	235	0.58	0.49	0.030	5.8
	B1937+21	52403.3	900	1380	80	512	35.0	25.6	576	0.31	0.26	0.016
J2145–0750	52223.7	1500	860	40	256	19.7	102.4	91	0.38	0.32	0.020	1.2
	52232.9	3600	1380	80	512	4.4	102.4	222	0.21	0.18	0.011	0.92

¹: $M_{\text{max}} = 24576$ ²: $M_{\text{max}} = 81920$

in the frequency domain) might be indicated. This is often necessary in the analysis of simultaneous multi-observatory data sets due to the employment of different sampling intervals, and may also become important in future high-resolution studies of close-orbit binary pulsars where the apparent period can change significantly over the course of an observation. We suggest the technique be investigated as a means for avoiding the deleterious effects of time-domain re-sampling noticed by Karastergiou et al. (2001)⁴.

In theory, the above procedure allows absolute alignment in longitude of observations at different epochs and frequencies. In practice, the published dispersion measure may derive from arbitrary profile alignment procedures, and previously published timing ephemerides may not extrapolate beyond the date range from which they derive accurately enough for phase alignment between different epochs. For these reasons, we did not attempt absolute alignment, and our longitude axes include an arbitrary offset.

2.3. Accumulation of Statistics

The first step of processing after forming the longitude/time array was to correct for an absolute offset due to the system noise power. To reduce the effect of slow variations in the system temperature we subtracted a running baseline, computed as the mean over the surrounding ± 1000 pulses of all samples in a defined “off-pulse” longitude interval. Denoting the result as S_{ij} where i and j are indices in pulse longitude and pulse num-

ber, we then computed the (normalized) average pulse profile as

$$\mu_i = \frac{1}{N} \sum_{j=0}^{N-1} S_{ij}, \quad (1)$$

where N is the number of pulses analyzed. For convenience, at this point we re-normalized S_{ij} so that the peak bin of μ_i had a value of 1. We then computed a version of the data from which the average profile was subtracted:

$$S'_{ij} = S_{ij} - \mu_i. \quad (2)$$

The remaining analysis involved the integration of three kinds of correlation statistics that differ in their treatment of the longitude dimension. These are the full two-dimensional autocorrelation function (2DACF), the longitude-resolved autocorrelation function (LRACF) and the longitude-resolved cross-correlation function (LRCCF).

To examine the autocorrelation statistics of the signal while keeping computational time and space requirements manageable, we divided the input pulse series into N/M M -pulse blocks of data and obtained estimates of the fluctuation power spectra (LRFS and 2DFS) by averaging the results of N/M individual spectra computed from the squared modulus of the appropriate DFTs. By application of the Wiener-Khinchin theorem, the corresponding autocorrelation functions were obtained via the DFTs of the power spectra. The choice of M affected our sensitivity to nearly coherent modulation: since beyond this length we summed *power* spectra, signals with decorrelation time-scales longer than M pulses would have been detected with reduced significance. Signals with decorrelation timescales shorter than M could also have suffered since in that case the response would be spread over several coefficients,

⁴ Although we also note that for some purposes, including application of the LRCCF between observatories as in Karastergiou et al. (2001), the synthesis of synchronous samples is unnecessary and should be avoided.

however here the sensitivity can be recovered by smoothing the power spectrum. Our approach was therefore to choose the largest M that was practical given the computational and memory requirements.

In computation of the LRFS, each one-dimensional spectrum was obtained using the squared modulus of the coefficients of DFTs performed along a constant-longitude column of the longitude/time array:

$$\text{LRFS}_{ij}^{\text{raw}} = \frac{1}{N} \sum_{k=0}^{N/M-1} \left| \sum_{l=kM}^{(k+1)M-1} S'_{i,l} e^{-2\pi j l \sqrt{-1}/M} \right|^2. \quad (3)$$

To remove the effect of the variance of the system noise, including non-white components due to interference and system temperature variations not removed in the pre-processing stages, we subtracted from each element of the spectrum the corresponding value from the mean fluctuation spectrum of all designated “off-pulse” longitude bins, dropping the superscript of Eq. 3 to denote the noise-corrected LRFS.

We then performed DFTs along constant-longitude columns of the LRFS to obtain the LRACF. To avoid performing a cyclic convolution, the individual LRFS were actually computed over $2M$ points, of which the elements of one contiguous half were set to zero. The resulting LRFS elements are not independent, so to facilitate proper evaluation of the significance of spectral features, after using it to form the LRACF we discarded the odd-numbered coefficients of the LRFS (which has the same result as an M -point transform of the non-padded data). To correct the LRACF result for edge normalization effects we divided the result by $1 - j/M$, where j is the lag number. The result is:

$$\text{LRACF}_{ij} = \frac{1}{N(1 - j/M)} \sum_{k=0}^{N/M-1} \sum_{l=kM}^{(k+1)M-1-j} S'_{il} S'_{i(l+j)}. \quad (4)$$

The zero lag of the LRACF gives the longitude-resolved variance:

$$\sigma_i^2 = \text{LRACF}_{i0} \quad (5)$$

$$= \frac{1}{N} \sum_{j=0}^{N-1} (S'_{ij})^2. \quad (6)$$

From this we computed the modulation index as $m_i = \sigma_i / \mu_i$. Since the zero lag of the LRACF is simply the sum of all elements of the corresponding fluctuation power spectrum, we may view the variance in a given longitude bin as having contributions from different frequencies (Parseval’s theorem). We made use of this fact to compute modulation indices with the exclusion of the lowest frequency bin, since it often contained a strong component which, by virtue of its low frequency and longitude-independent modulation index, we attribute to interstellar scintillation.

The 2DFS was derived through a similar division of the data sequence into M -pulse blocks. Since it integrates in longitude, we only include a designated on-pulse longitude interval in the analysis. The squared modulus of the two-dimensional DFT of such blocks gives the 2DF power spectrum, which was

integrated over all blocks:

$$2\text{DFS}_{ij}^{\text{raw}} = \frac{1}{NB} \sum_{k=0}^{N/M-1} \left| \sum_{l=kM}^{(k+1)M-1} \sum_{b=0}^{B-1} S'_{i,l} e^{-2\pi \sqrt{-1}(ib/B + jl/M)} \right|^2, \quad (7)$$

where B is the number of longitude bins. When possible, to correct for the autocorrelation characteristics of the noise and interference, the raw 2DFS of an equal-sized “off-pulse” longitude interval (or the mean from several intervals) was computed and subtracted from the raw on-pulse spectrum.

The 2DFS has two dimensions that are both dimensionless frequencies. In this work we refer to quantities in the pulse number- and longitude-associated axes as temporal and longitudinal frequencies respectively, and plot the spectra with the longitudinal frequency axis as the abscissa. We usually use units of (subpulse) cycles per (spin) period (cpp) for these quantities, which in the case of longitudinal frequencies also corresponds to degrees of subpulse phase per degree of longitude. The 2DFS is periodic (due to aliasing with the finite sample interval) and symmetric about the diagonal (due to the real-valued input), obeying the relation $2\text{DFS}_{ij} = 2\text{DFS}_{(\pm i + cB)(\mp j + dM)}$ where c and d are arbitrary integers, and can therefore be fully specified by computing a contiguous region of either $B/2 + 1 \times M$ coefficients, or $B \times M/2 + 1$ coefficients. In this work we plot the region given by $i \in [-B/2 : B/2]$ (i.e. longitudinal frequencies between $-180^\circ/\Delta\phi$ and $180^\circ/\Delta\phi$, where $\Delta\phi$ is the longitude sampling interval) and $j \in [0 : M/2]$ (i.e. temporal frequencies between 0 and 0.5 cpp), which generally avoids having responses “wrap” across borders in the planar projection, and directly gives information concerning the apparent sense and rate of any subpulse drift pattern.

The two-dimensional DFT of the 2DFS gives a form of Two-Dimensional Autocorrelation Function (2DACF), a function which, like the LRFS, has seen frequent use in the past for drifting subpulse analysis (e.g. Taylor et al. 1975). Again, it is important to pad the data with zeroes (in both axes) to avoid computing a cyclic convolution, and to discard odd-numbered rows and columns of the resultant 2DFS to avoid misinterpreting the significance of spectral features. The correction for edge normalization effects was performed through multiplication by $1 - j/M$; since the pulsar signal is not expected to extend beyond the longitude boundaries, additional normalization by $1 - i/B$ is not appropriate. The result is:

$$2\text{DACF}_{ij} = \frac{1}{NB(1 - j/M)} \sum_{k=0}^{N/M-1} \sum_{l=kM}^{(k+1)M-1-j} \sum_{b=0}^{B-1} S'_{bl} S'_{(b+i)(l+j)}. \quad (8)$$

The zero pulse-number lag of the 2DACF gives the single-pulse ACF used by Jenet et al. (2001):

$$\text{ACF}_i = 2\text{DACF}_{i0} \quad (9)$$

$$= \frac{1}{N} \sum_{j=0}^{N-1} \sum_{b=0}^{B-1} S'_{bj} S'_{(b+i)j}. \quad (10)$$

As an additional diagnostic of pulse-to-pulse correlations, we computed the LRCCF, which measures the covariance between every pair of longitude bins as a function of pulse number offset. We define the LRCCF as

$$\text{LRCCF}_{i_1 i_2 k} = \frac{1}{N-k} \sum_{j=0}^{N-k-1} S'_{i_1 j} S'_{i_2 (j+k)}. \quad (11)$$

Our definition differs somewhat from that of Popov (1986), who normalized by $1/\sigma_{i_1} \sigma_{i_2}$ to obtain a true correlation rather than a covariance. We find the covariance preferable in the evaluation of the significance of low S/N results since the noise levels are identical in all bins of each two-dimensional (i_1, i_2) map. The computation of the LRCCF could, in principle, be incorporated within the above scheme by integrating the conjugate product of complex LRFS pairs and taking the DFT of the result, however the computational complexity is much greater than for the autocorrelation techniques above. Since we were only interested in the first ~ 10 ($\ll M$) lags we found it more efficient to compute directly from Eq. 11. We note however that the frequency domain counterpart (the Longitude-Resolved Fluctuation Cross-Power Spectrum) could be useful in simultaneous multi-frequency observations for examining the presence, strength and relative phase of periodic modulations between different longitudes and frequencies.

Finally, although individual pulse detections were not the focus of this work, the assembled data set provides an opportunity for a survey of giant pulse behaviour in recycled pulsars. For this reason, we searched each observation for significant single pulses by convolving each pulse with boxcars of widths of 1, 2, 3, 4, 6, 8, 12 ... W_{\max} bins (where W_{\max} is approximately the width of the on-pulse region of the average profile) and selecting those pulses containing convolved samples with a single-trial significance exceeding 6σ . We then computed the energy of the selected pulses as the sum of intensity values over an interval centered on the same longitude as the detection boxcar but with twice the width, and expressed these as a fraction of the energy of the average profile.

3. Results

3.1. Non-Detections

In the observations of PSR J0218+4232, J0034–0534, J0613–0200, J1643–1224 and B1937+21, with the exception of very low frequency fluctuation attributable to scintillation, we found no detectable modulation in any of the measured statistics. As with all pulsars observed, this included searches of the LRFS for transform lengths from 2^9 to 2^{17} pulses (unless the number of pulses observed was less than this), from which one may derive limits on the presence of quasi-periodic modulation. Considering a longitude-resolved variance computed over a given interval $\Delta\nu$, the noise terms in the sum result in an approximately Gaussian distribution (central limit theorem) with a standard deviation proportional to $\Delta\nu^{1/2}$. For a given noise level estimated from the off-pulse parts of a LRFS, we take the square root of the $3\text{-}\sigma$ point of the noise in a given estimated variance (Eq. 6) as the minimum detectable standard deviation. These values are given for each observation in Table

1. The minimum detectable standard deviation for a given frequency integration is given by $\sigma_g(\Delta\nu/\text{cpp})^{1/4}$, which we have tabulated as σ_m for the full modulation index ($\Delta\nu = 0.5$ cpp) and for unresolved (i.e. nearly coherent) features in the longest transform, as σ_c ($\Delta\nu = 1/M_{\max}$ cpp, $M_{\max} = 2^{17}$ unless noted). With the exception of PSR B1937+21, the four pulsars for which we have not detected modulation are those with the worst detection limits, and for this reason the results cannot be taken as evidence for low modulation indices.

The search for bright individual pulses was successful in several pulsars (noted below), however with the exception of PSR B1937+21, no pulsar produced clearly detectable *giant* pulses in our observations. For PSR J0613–0200, one pulse barely exceeded the threshold, occurring within the (broad) on-pulse region, with an energy exceeding the mean by a factor of 20 and a width of one bin. Further studies should be made before attributing this detection to a giant pulse phenomenon. For all pulsars, the $6\text{-}\sigma$ energy limit for individual samples is presented in Table 1 as E_{\min} ; for wider pulses the limit scales as $n^{1/2}$ where n is the number of samples to add.

3.2. PSR J1012+5307

The fluctuation spectra for PSR J1012+5307 (Fig. 1) indicate the presence of quasi-periodic modulation in all three major profile components. Moreover, it is apparent in the 1380 MHz observation that the peak frequency of the modulation varies with longitude, showing different values in components Ia, Ib and II. To better examine the differences between the components, we have plotted fluctuation spectra from components Ia, Ib and IIb in Fig. 2. From this figure it is apparent that although the overall depth of modulation in component Ia is higher than that in Ib, its quasi-periodic feature is broader in frequency space. We also note the presence of narrow features in the spectra of components Ib and IIb at frequencies close to twice the frequency of peak power. The significance of these features deteriorates with a narrower smoothing function, indicating that their intrinsic width is close to that seen in Fig. 2.

We detected 70 individual bright pulses in the 1380 MHz observation, the strongest of which had an energy five times the mean pulse energy for this observation. The pulse profile formed by adding these pulses shows relatively more emission in components Ia and IIb compared to Ib and IIa, consistent with the higher modulation indices found in these regions.

The two-dimensional fluctuation spectra were contaminated by the presence of broad stripes aligned with the temporal frequency axis, which we were unable to subtract due to the lack of sufficiently wide off-pulse longitude intervals. Nevertheless, it is clear that the modulation power in the component I is divided between two main regions, one with zero frequency in the longitude axis, and one with a frequency of ~ -10 cpp (Fig. 3). The latter component indicates the presence of quasi-periodic drifting subpulses, with a longitude separation of $\sim 40^\circ$ between subpulses. Since the component I is double-peaked, one might also consider the alternative of longitude-stationary subpulse modulation with a simple phase offset between the two halves of the profile com-

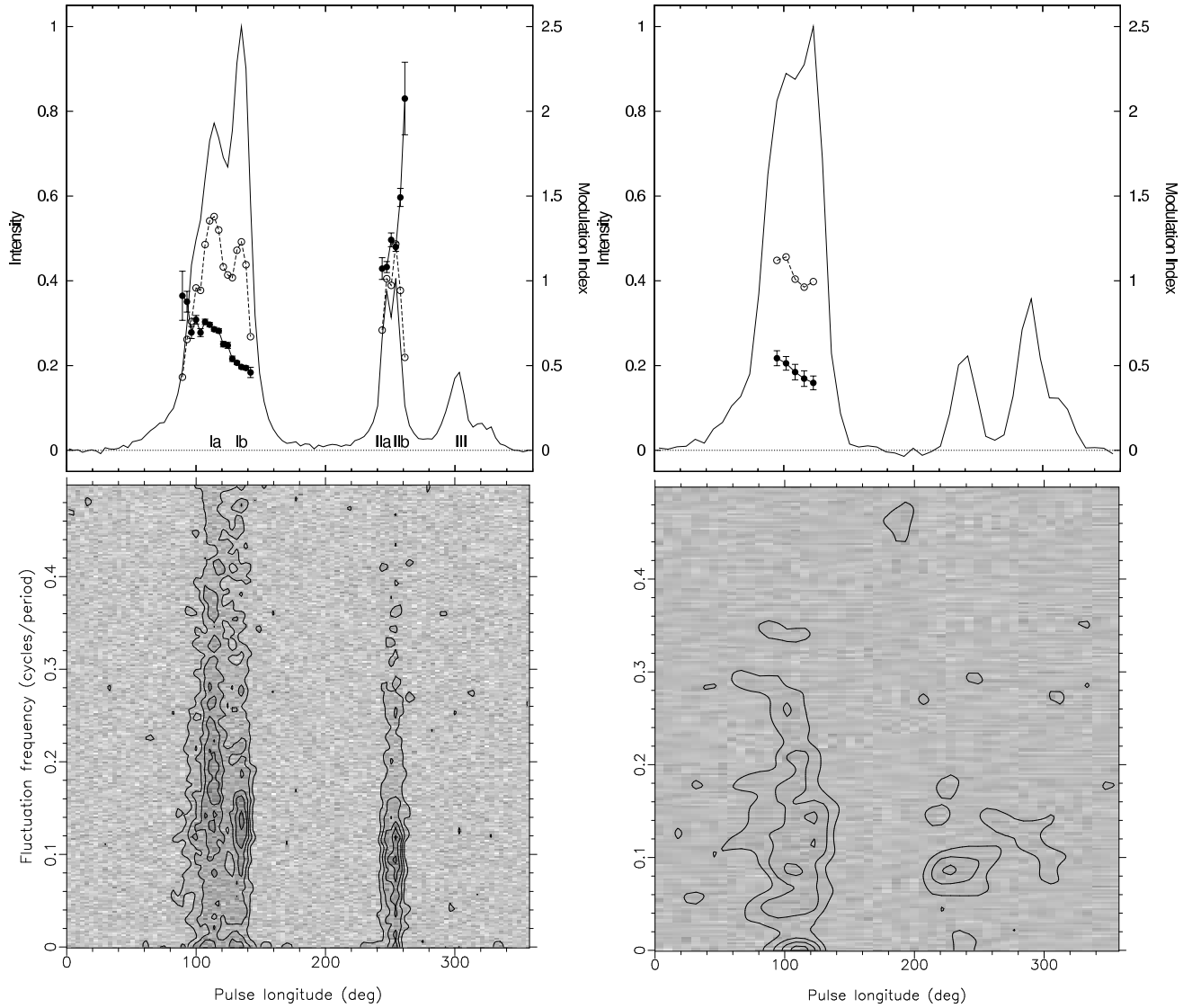


Fig. 1. Longitude-resolved modulation statistics for PSR J1012+5307 at 1380 MHz (left) and 840 MHz (right). Top panel: mean pulse profile (top, solid lines), standard deviation (unfilled circles) and modulation index (filled circles, right-side axis scales) for PSR J1012+5307 at 1380 MHz (left) and 840 MHz (right). The names used for components are indicated in the top left panel. The standard deviation and modulation index are subject to a $3\text{-}\sigma$ threshold in the power values from which they are derived, to ensure their significance. A strong component in the DC frequency bin of the LRFS is attributed to scintillation and was not included in the calculation of these statistics. Bottom panel: LRFS, shown as a greyscale computed with $M = 512$, along with contours of Gaussian-smoothed version of the same spectrum of FWHM $0^\circ \times 0.02$ cpp (1380 MHz) and $20^\circ \times 0.02$ cpp (840 MHz).

ponent. However, this can be rejected because the peak frequency obtained could not be more than 180° divided by the component separation of $\sim 40^\circ$, i.e. ~ 5 cpp, where there is certainly no peak in the spectrum. The spectral component centered around zero longitudinal frequency indicates the presence of longitude-stationary quasi-periodic modulation, while its relatively narrow extent suggests it extends across most of the component I.

It is conceivable that the two spectral components in the 2DFS are in fact associated with with same modulation feature, if the apparent temporal frequency offset is actually spurious. In this case the shifted, double-peaked nature of the spectrum in the longitudinal axis is indicative of linear drifting with a

frequency of ~ 5 cpp and a phase step between opposite halves of the profile component (Edwards et al. 2003).

3.3. PSR J1022+1001

This pulsar showed non-periodic modulation at 328, 840 and 1380 MHz (Fig. 4). At 1380 MHz, the trailing component is seen to be very strongly modulated, a fact corroborated by the dominance of this component in the average profile derived from the $\sim 10^4$ individual pulses we detected. In this observation, the brightest pulses had an energy ~ 6.5 times the mean, while the distribution of energy measured in a longitude in-

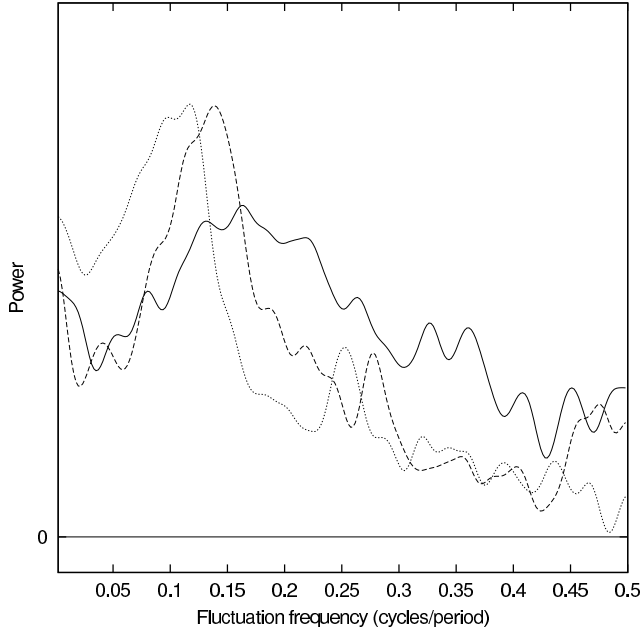


Fig. 2. Fluctuation spectra for PSR J1012+5307 at 1380 MHz, from peak bins in components Ia (solid), Ib (dashed) and Iib (dotted; Iia appeared similar and is omitted for clarity). The raw spectra were convolved with a Gaussian of FWHM 0.02 cpp before plotting.

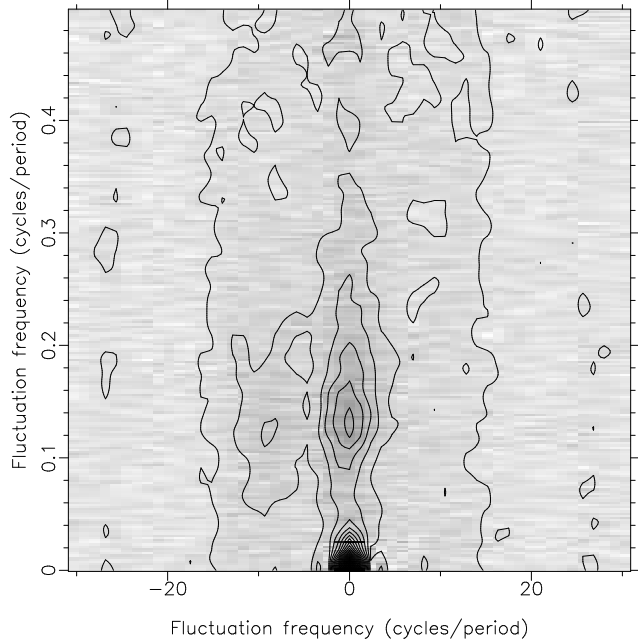


Fig. 3. 2DFS for component I of PSR J1012+5307 at 1380 MHz, using $M = 512$ (greyscale) and smoothing by convolution with a Gaussian of FWHM 0×0.02 cpp (contours).

interval spanning the trailing component was consistent with an exponential or power-law.

The fluctuation spectra of the bins near the two peaks of the average profile at 1380 MHz are shown in Fig. 5. While the leading component shows a flat fluctuation spectrum, the trailing component proceeds smoothly to a maximum at the

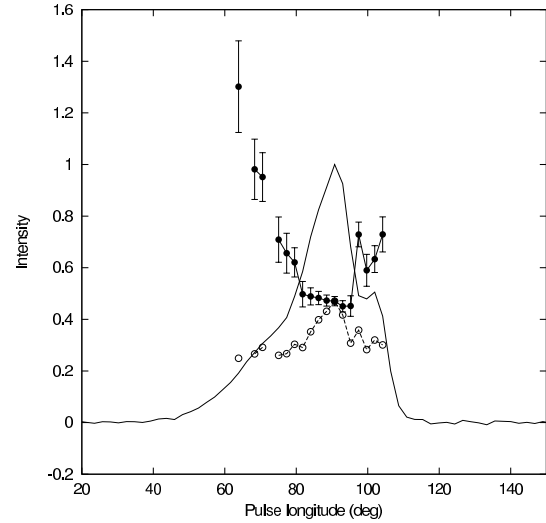
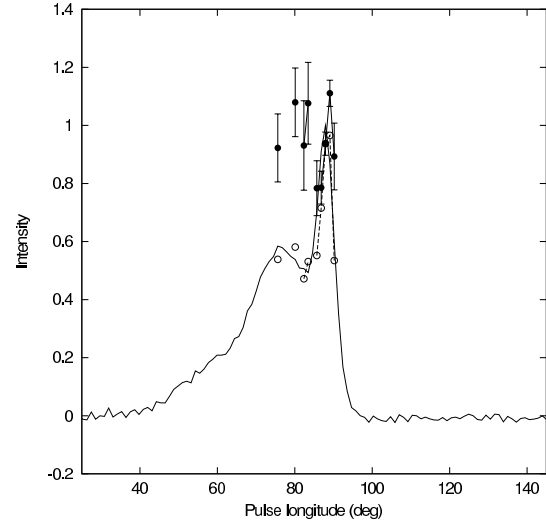
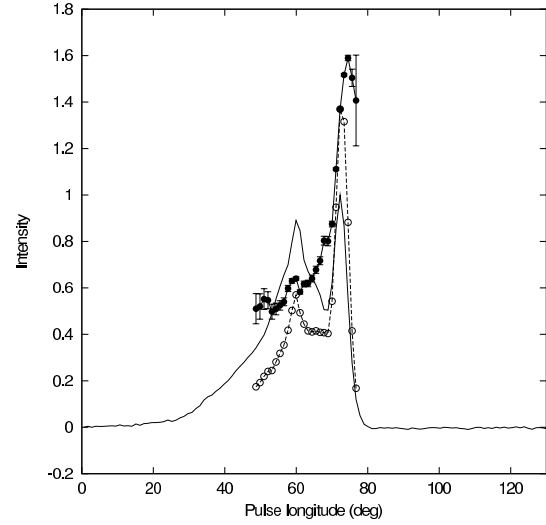


Fig. 4. Average profile, standard deviation and modulation index for PSR J1022+1001 at 1380 (top), 840 (middle) and 328 MHz (bottom). See caption for Fig. 1, but here the modulation index is plotted with the same scale as the other quantities.

Nyquist frequency. This corresponds in the autocorrelation function to a strong negative spike at a lag of one pulse. There

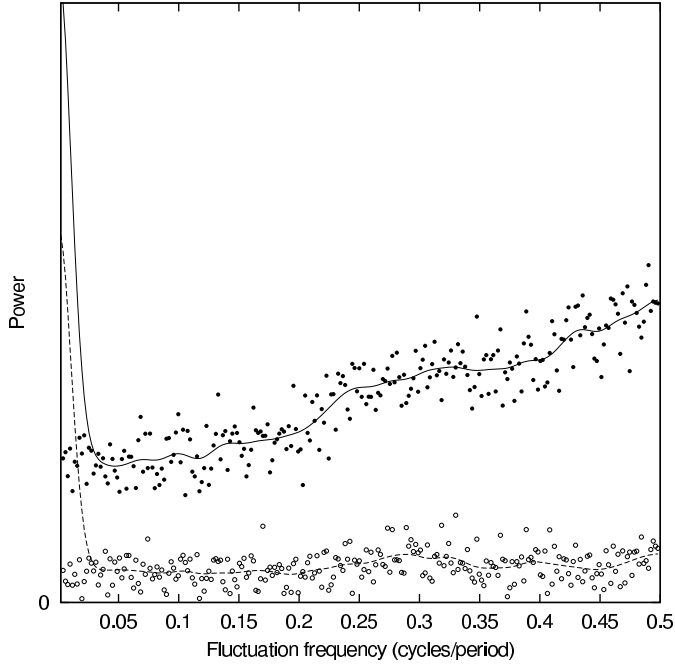


Fig. 5. Fluctuation spectra from peak longitude bins of the leading (open circles, dashed line) and trailing (filled circles, solid line) components of PSR J1022+1001. The points show the measured spectrum ($M = 512$) in the peak bin, while the solid and broken lines show the spectra from the peak and surrounding bins respectively, after smoothing by convolution with a Gaussian of FWHM 0.02 cpp. The low-frequency excess is due to very low frequency modulation (attributed to scintillation), broadened by the Gaussian smoothing kernel.

is no evidence for any periodicity associated with this correlation.

3.4. PSR J1518+4904

We detected quasi-periodic modulation throughout the double-peaked main profile component of PSR J1518+4904 (Fig. 6), with a frequency of approximately 0.38 cpp. In the peak bin this modulation contributes about half of the total modulation power, however this fraction decreases significantly toward the trailing part of the profile. The 2DFS (Fig. 7) shows a corresponding component with its peak centered at a longitudinal frequency ~ -10 cpp, corresponding to a phase slope of about half a cycle across the pulse window. The 2DACF (Fig. 8) confirms this description, showing the characteristic repeating pattern of drifting subpulses. The fact that for any given pulse number lag the 2DACF is singly-peaked confirms what one might expect with the relatively small phase slope, namely that usually only one subpulse is present as part of the quasi-periodic pattern. Fig. 9 shows this more clearly for the zero lag, and confirms that the subpulses are significantly narrower than the average profile. The drift pattern is also manifest in the LRCCF (Fig. 10), from which it is clear that drifting of the modulation applies over the entire longitude window defined by the average profile.

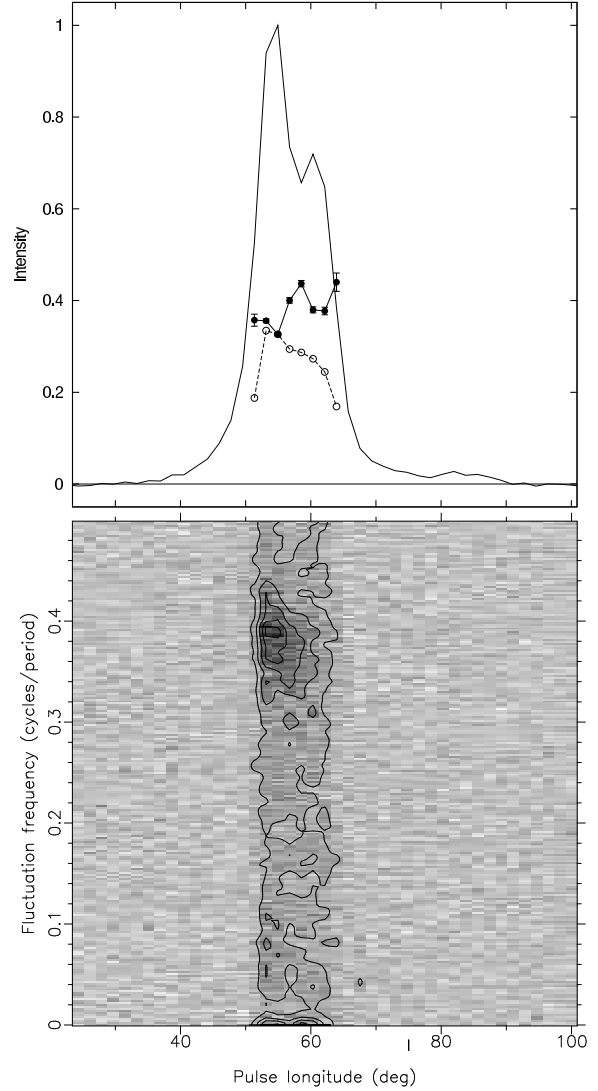


Fig. 6. Longitude-resolved statistics for PSR J1518+4904. See caption for Fig. 1.

We detected 1650 individual pulses from this pulsar, the brightest of which had an energy 4.8 times the mean.

3.5. PSR J1713+0747

We have detected modulation in observations at PSR J1713+0747 from 840 to 2240 MHz (Fig. 11). The evolution in the pulse profile and modulation index is very minor over this range, however to aid in the assessment of the longitude-dependence of the modulation index under the low longitude resolution available, we have provided plots for all four frequencies. It is clear that the leading edge shows a higher modulation index than other parts of the profile. A selection of one-dimensional fluctuation spectra are shown in Fig. 12. Two broad maxima at frequencies of ~ 0.17 and ~ 0.35 cpp are clearly seen.

We detected ~ 50 individual pulses at 1190 MHz, with energies up to 6 times the mean.

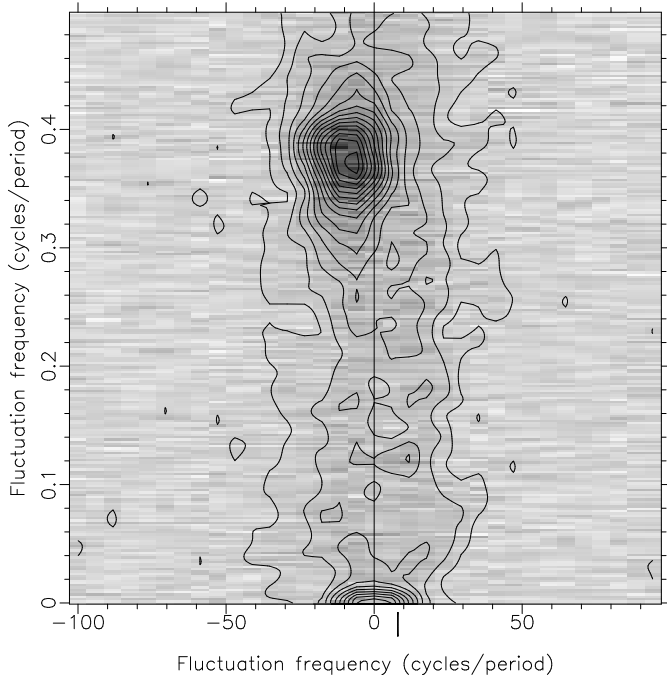


Fig. 7. 2DFS for PSR J1518+4904 at 1355 MHz. See caption for Fig. 3.

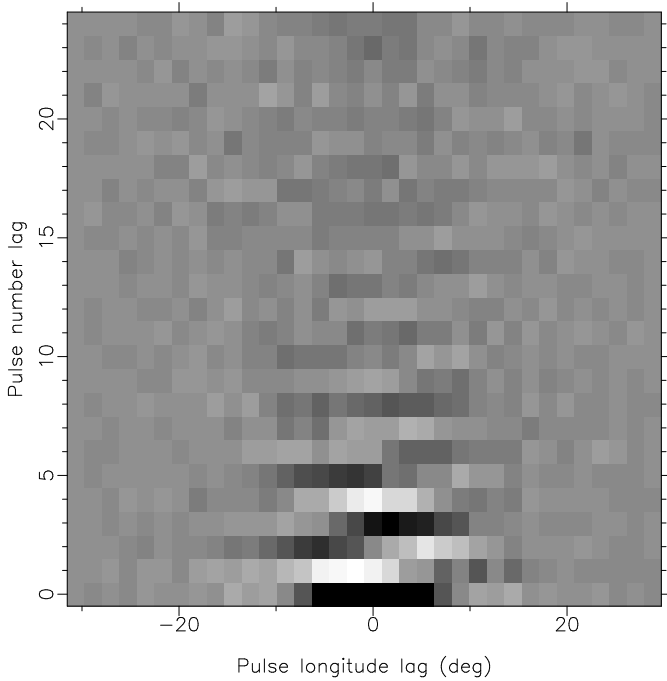


Fig. 8. Lags 0–24 of 2DACF for PSR J1518+4904 at 1355 MHz. Black and white values correspond to the most positive and negative values respectively, outside the zero lag.

3.6. PSR J1918–0642

We detected modulation in the strongest two longitude bins in an observation of PSR J1918–0642 at 1380 MHz (Fig. 13). There is some evidence for a concentration of power between 0.25 – 0.5 cpp in the fluctuation spectrum (Fig. 14), however the limited sensitivity makes this result uncertain.

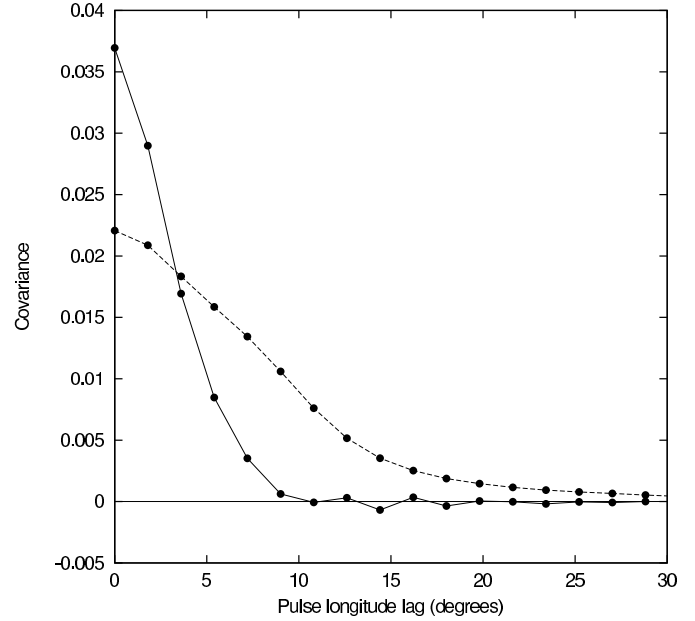


Fig. 9. Single-pulse ACF (solid line) and ACF of the average profile (dashed line) for PSR J1518+4904 at 1355 MHz.

3.7. PSR J2145–0750

In observations at 860 and 1380 MHz, this pulsar showed strong intensity fluctuations, at some pulse longitudes exceeding 100% (Fig. 15). Two 1380-MHz observations provided sufficient sensitivity to detect weak quasi-periodicities around ~ 0.22 and 0.45 cpp, we plot the result from the better observation in Fig. 16. To check for stationary or drifting modulation in the extended bridge and trailing component, we computed the 2DFS of this longitude interval. No evidence for quasi-periodicity was found, but very broad features such as those seen in the peak bins cannot be ruled out. In the 1380 MHz observation we detected 490 individual pulses, the strongest of which had an energy 3.7 times the mean. The profile formed by adding these pulses was dominated by a narrow component around pulse longitude 215° , indicating that intensity enhancements in this component are not accompanied by enhancements at other longitudes. The less sensitive 840 MHz observation yielded similar results for the 11 detected pulses.

4. Discussion

The results of this study show that the emission from recycled pulsars strongly varies on timescales comparable to the rotation period. Of the seven pulsars for which we were sensitive to (aperiodic) modulation with $m > 0.5$, we detected such modulation in all but one (PSR B1937+21). Quasi-periodicities also seem to be a common feature of the fluctuation spectra, however features are typically broad and often do not comprise the dominant contribution to the observed modulation index. Such a broad, weak feature has also been observed in PSR J0437–4715 (Vivekanand et al. 1998).

For PSR J1012+5307 and PSR J1518+4904 the presence of offset components in the two-dimensional fluctuation spectra indicates that the phase of the quasi-periodic modulations

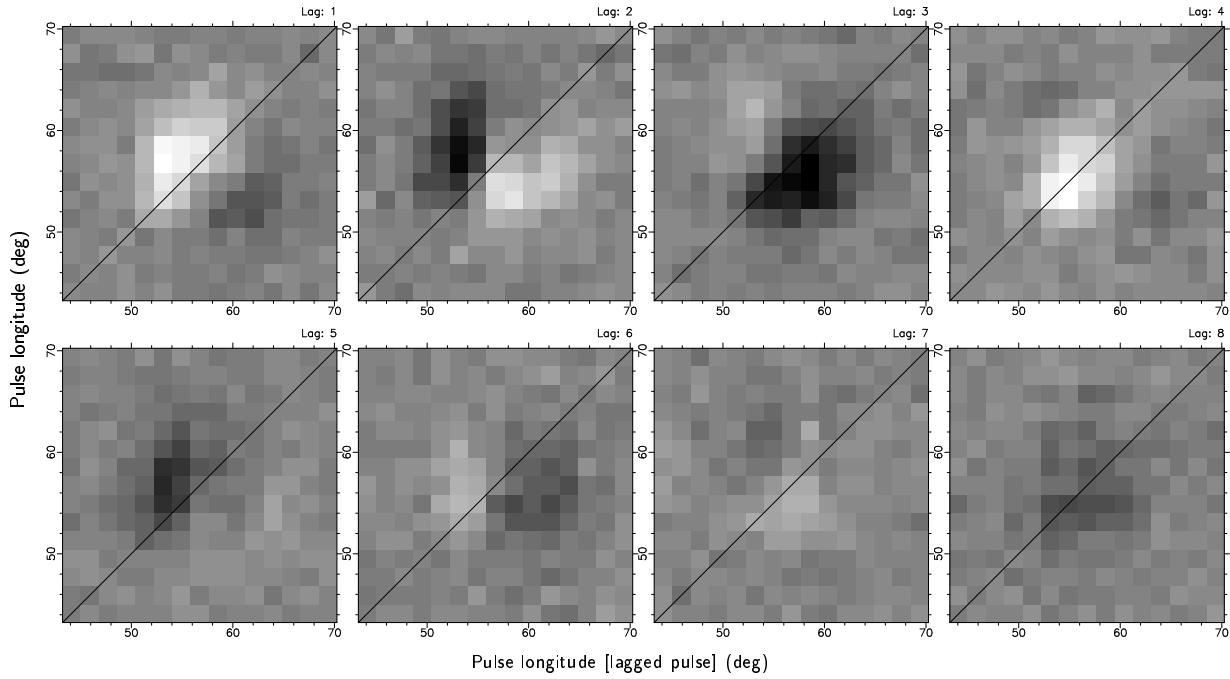


Fig. 10. Lags 1–8 of LRCCF for PSR J1518+4904 at 1355 MHz. Grey levels are set as in Fig.8. The solid lines connect bins with the same longitude value in the lagged and non-lagged pulse (i.e. the autocorrelations).

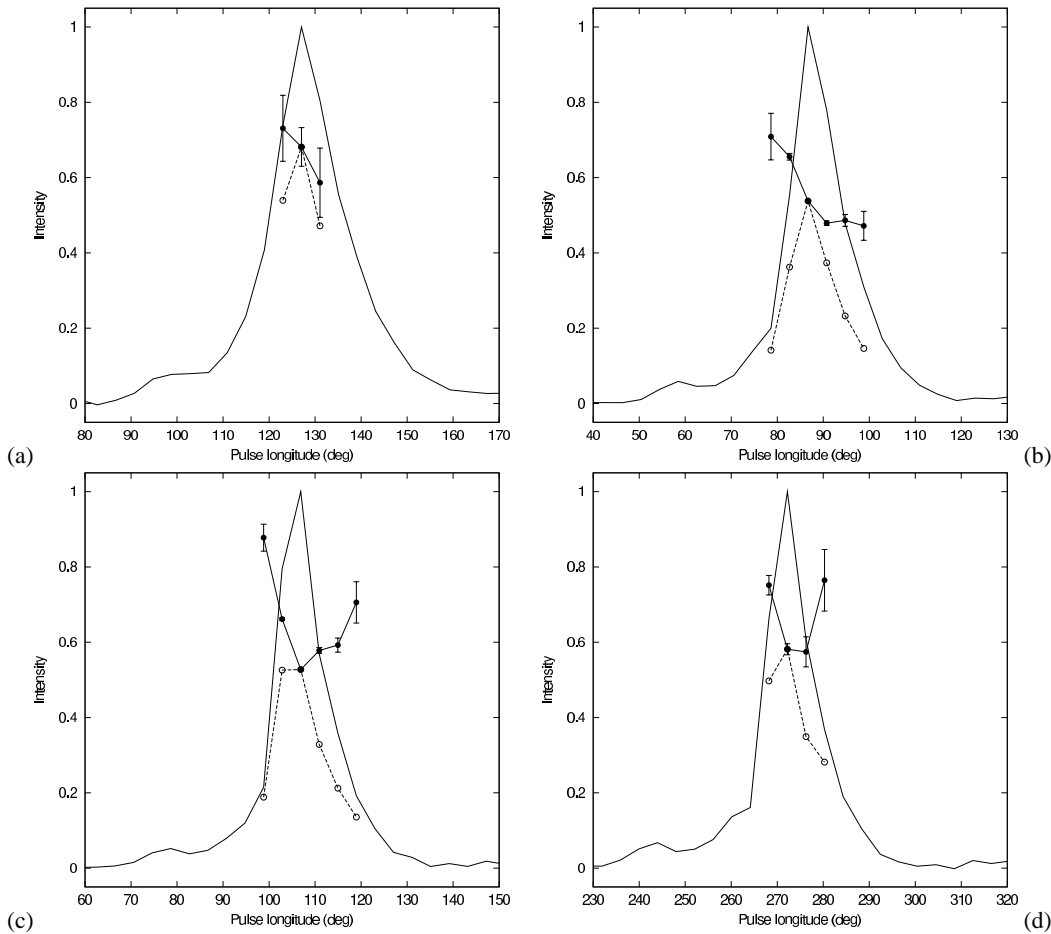


Fig. 11. Average profile, standard deviation and modulation index for PSR J1713+0747 at (a) 840 MHz, (b) 1190 MHz, (c) 1700 MHz and (d) 2240 MHz. See also caption for Fig. 1.

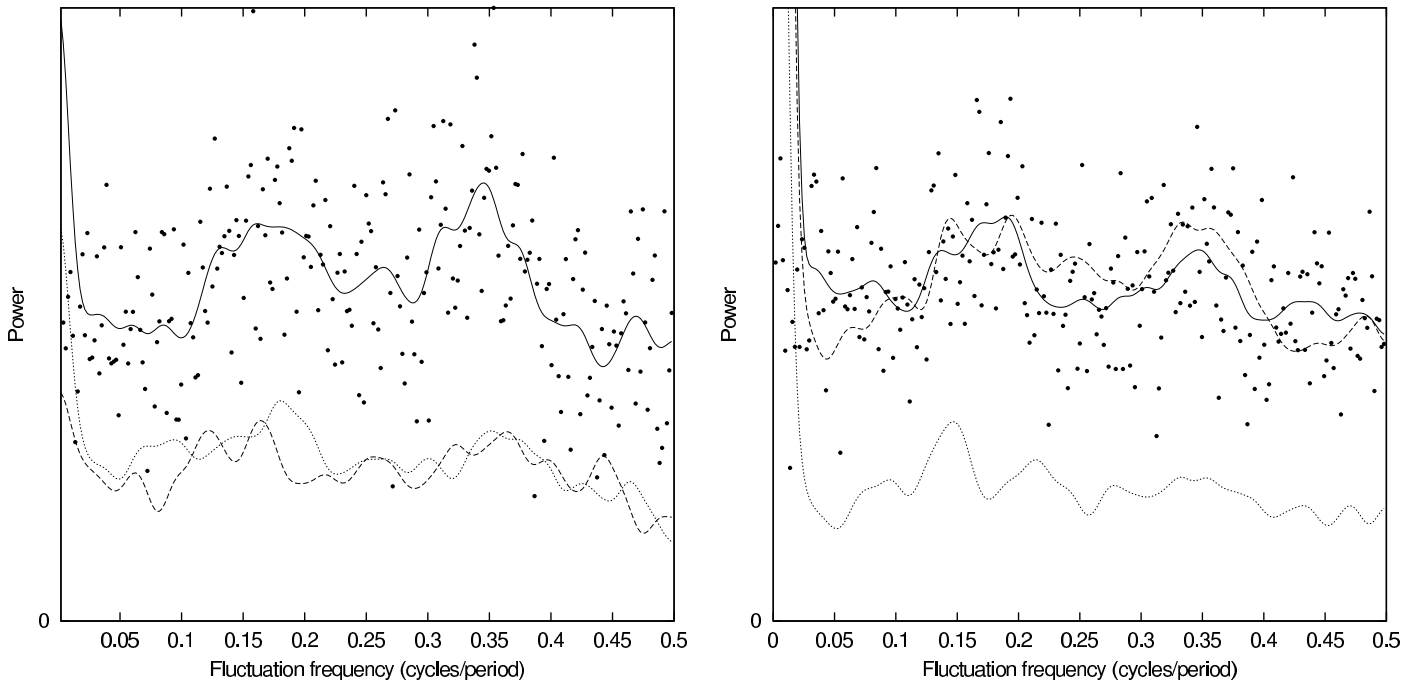


Fig. 12. Fluctuation spectra from significant bins of the LRFS, at 1190 MHz (left) and 1700 MHz (right), for PSR J1713+0747. See also caption for Fig. 5.

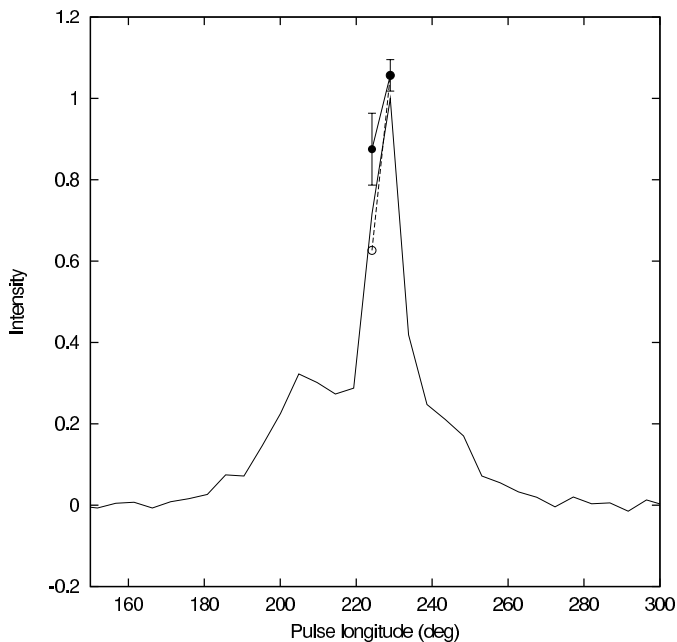


Fig. 13. Average profile, standard deviation and modulation index for PSR J1918-0642 at 1380 MHz. See caption for Fig. 1.

advances from the leading edge to the trailing edge of the main profile component. That is, the components of the emission that are periodically modulated appear at successively later longitudes. In addition to the results presented here, we checked other observations and found similar behaviour. These are the first ever detections of drifting subpulses in recycled pulsars. For the other pulsars the sensitivity to modulation at longitudes

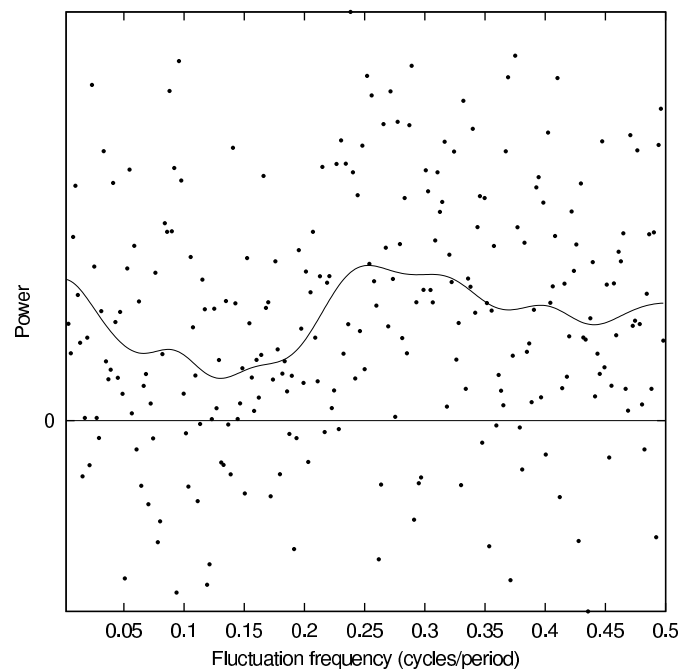


Fig. 14. Fluctuation spectrum from the peak longitude bin of PSR J1918-0642, at 1380 MHz. A Gaussian of FWHM 0.05 cpp was used to produced the smoothed spectrum. (See caption for Fig. 5.)

away from the peak is probably too poor to have allowed detection of similar phenomena, if present. For PSR J0437-4715 the sensitivity achieved by Vivekanand et al. (1998) appears more than sufficient to have ascertained whether the modulation drifts, but unfortunately the two-dimensional autocorrela-

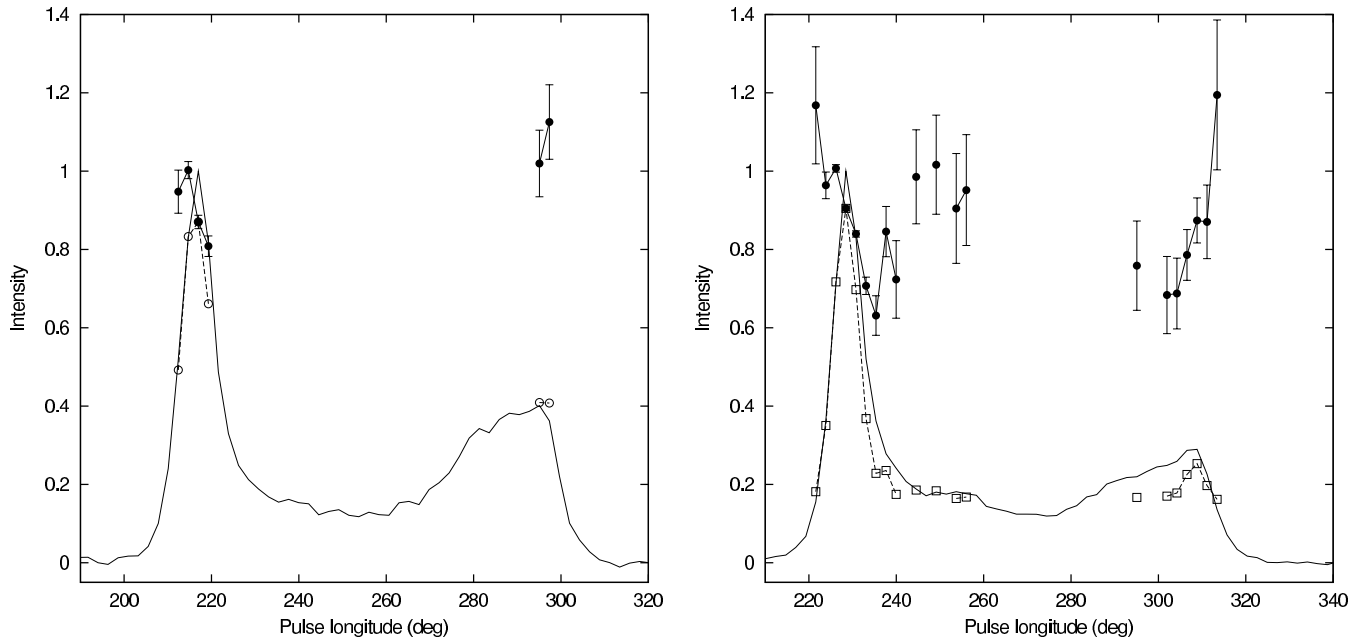


Fig. 15. Longitude-dependent statistics for PSR J2145–0750 at 860 MHz (left) and 1380 MHz (right). See caption for Fig. 1.

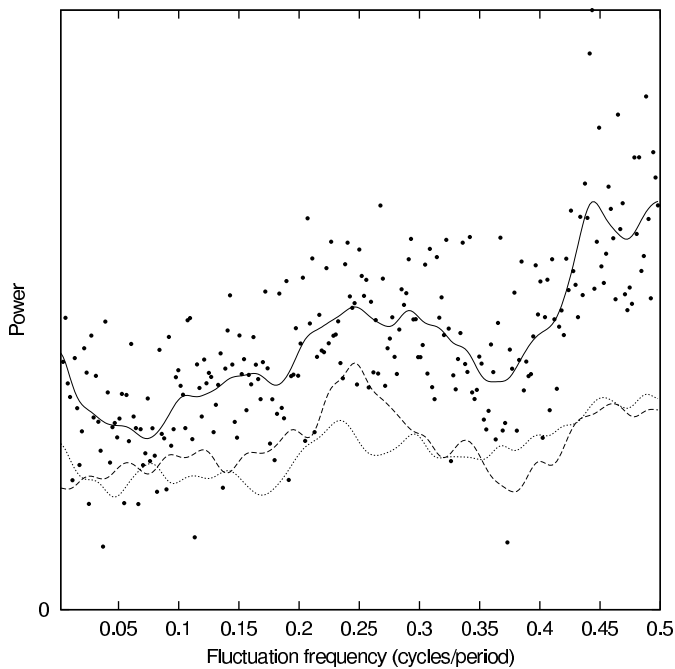


Fig. 16. Fluctuation spectrum from the peak longitude bin (solid line) and the bins immediately before (dashed) and after (dotted) it, for PSR J2145–0750, at 1380 MHz. See caption for Fig. 5.

tion function was computed without prior subtraction of the average profile, causing it to be dominated by this component and potentially making any weak drift pattern invisible in the plot. Determining whether or not the subpulse modulation drifts would provide a good test of the model of Gil & Krawczyk (1997), which predicts stationary modulation.

Despite the very different physical conditions in the polar cap regions and magnetospheres of recycled pulsars versus ordinary pulsars, the observed single-pulse phenomena are broadly consistent. Specifically, like ordinary pulsars they tend to have modulation indices of 0.5–1.5 (cf. Taylor & Huguenin 1971; Bartel et al. 1980; Weisberg et al. 1986) and non-white fluctuation spectra (cf. Taylor & Huguenin 1971; Backer et al. 1975). Rankin (1986) distinguishes between modulation in so-called conal and core components of the emission, noting that conal components frequently show quasi-periodic modulation with periods of 2–10 pulses, which can sometimes be highly coherent, while core components tend to possess weak, broad low frequency excesses or peaks in their fluctuation spectra⁵. We clearly do not detect any features of high coherence in the recycled pulsars studied here, however it is difficult to say what proportion of normal pulsars show them, for studies have tended to favour pulsars known to possess them over those with broad components that are more difficult to characterize. None of the pulsars studied here appears to show a low-frequency excess (except for the very low frequency scintillation components), perhaps indicating that recycled pulsar emission is not related to core emission in slow pulsars.

An apparent exception to the above generalizations is PSR B1937+21. Our non-detection ($m < 0.26$) is consistent with the previously measured modulation index of 0.18 (Jenet et al. 2001)⁶. The reported constancy of the modulation index with longitude (except for the trailing edge, where giant pulses oc-

⁵ Rankin (1986) draws attention to a number of reports of low-frequency quasi-periodicities in core-associated emission ($P_3 \sim 20$ pulses), however examination of the source literature (or at least, those that published their spectra) indicates that with some exceptions, most are just as consistent with a low frequency excess as with quasi-periodicity.

⁶ Since Jenet et al. (2001) dealt with baseband samples, the observed variance included the radiometer noise of the pulsar sig-

cur) suggests scintillation as a possible origin for the modulation, and Jenet et al. (2001) show that the level of modulation is consistent with the known properties of diffractive scintillation in this source. Jenet et al. (2001) use this result and the similarity of the single-pulse ACF to the ACF of the average profile to argue that the intrinsic emission of PSR B1937+21 is very stable, in contrast to all previously studied pulsars. However, Weisberg et al. (1986) find that pulsars they classified as “core” had low modulation indices, and indeed their result for PSR B2053+36 resembles that of PSR B1937+21 not only in the low value of modulation index but also in its constancy across most of the profile and in the shape of the profile itself. The issue could be resolved by examining the frequency structure of the modulation seen in these pulsars.

In ordinary pulsars, the presence of drifting subpulses is usually associated with a viewing geometry that traces the emission along a quasi-transverse path near the edge of the beam (e.g. Rankin 1986). This is consistent with the picture put forth by Ruderman & Sutherland (1975) that the pulsar beam consists of a circulating ring of subbeams corresponding to such a pattern of spark activity on the polar cap. The observation that drifting subpulse patterns are coherent between different pulse longitudes and between observations made simultaneously at different radio frequencies (i.e. that the temporal period P_3 is independent of these; see e.g. Taylor et al. 1975) lends strong support to this claim, as does the recent apparent detection of modulation at the circulation period in PSR B0943+10 (Deshpande & Rankin 2001). The presence of fluctuation components at different temporal frequencies ought, in such a model, to obey a mirror symmetry between pulse longitude pairs that sample the same part of the rotating subbeam system. A clear example of this is PSR B1237+25, where the relative importance of the (at least) three modulation features shares the same approximate symmetry in longitude as the average profile (Backer 1973).

How PSR J1012+5307 fits into this picture, if at all, is unclear. Taken at face value, the variation of peak fluctuation frequency with pulse longitude implies that components Ia, Ib and II all correspond to different (nested) rotating subbeam cones. The much higher modulation index of component II versus component I would support this assertion. In this case one might expect that the emission from 290 to 340° corresponds to the complementary components required to preserve symmetry mentioned above and ought to show a progression from low to high fluctuation frequencies with longitude (i.e. in reverse to that seen from Ia to Ib to II).

The detections of individual bright pulses made here are also broadly consistent with the behaviour of ordinary pulsars, the pulse energy distributions of which typically extend to a factor of a few higher than the mean (e.g. Ritchings 1976). A similar result for PSR J0437–4715 was presented by Jenet et al. (1998). With the exception of PSR B1937+21,

for which giant pulses are already known to occur, and PSR J0613–0200, for which the result of a single detection needs further investigation, we did not detect any giant pulses. If any of the pulsars observed had produced unresolved giant pulses with the same energy probability distribution as that reported for PSR B1937+21 at 430 MHz (Cognard et al. 1996), we should have detected in the worst case (PSR J0218+4232) ~ 90 of them. The results of Kinkhabwala & Thorsett (2000) appear to indicate that for PSR B1937+21, giant pulses are less frequently observed at higher frequencies, although they do not provide a fit to the probability distribution. Our rough estimate based on Fig. 8 of Kinkhabwala & Thorsett (2000), given a mean flux density of 10.4 mJy (from the spectral fit of Foster et al. 1991) and a ratio of 0.68:0.32 in energy between the main pulse and interpulse (measured from our observations) is that giant pulses of energies exceeding a given multiple of the mean energy occur of the order of 30 times less often at 1420 MHz than at 430 MHz. Giant pulses with a similar probability distribution would have been detected if present in any of the other pulsars observed. This result is particularly interesting for the first three pulsars listed in Table 1, since among field recycled pulsars the inferred magnetic field strengths at the light cylinder for these pulsars are exceeded only by those of PSRs B1937+21 and B1957+20, making them prime candidates for giant pulses according to Cognard et al. (1996).

Other than the detections of giant pulses in PSR B1937+21 and PSR B1812–24, we note that there exist in the literature largely unexamined reports of strong pulses from PSR B1534+12 (Sallmen & Backer 1995; Sallmen 1998). The pulse energy distribution clearly extends to much higher energies than observed here for other recycled pulsars (except PSR B1937+21), with the version given by Sallmen (1998) depicting the detection of pulses up to 17 times the mean energy, from a sample of just 12000 pulses. One wonders whether, were a data set of a number of pulses comparable to those used in studies of PSR B1937+21, PSR B1821–24 and the Crab pulsar analyzed ($\sim 10^7$), sufficiently bright pulses would be received for them to be considered “giant”. Such a result would be very interesting, since the inferred magnetic field strength at the light cylinder for PSR B1534+12 is low compared to most recycled and young pulsars ($\sim 1.6 \times 10^3$ G, versus $\sim 10^6$ G for PSR B1937+21 and $\sim 9 \times 10^5$ G for the Crab pulsar). The suggestion of Cognard et al. (1996) that this parameter is an indicator of giant pulse activity could be strongly tested by studying strong pulses from PSR B1534+12.

Given the lack of a complete theory of pulsar emission, there are few predictions that can be tested by the new observations presented here. A recent attempt at a systematic prescription for the properties of emission as a function of pulsar parameters for both normal and millisecond pulsars is that of Gil & Sendyk (2000). They postulate that the polar gap region is populated by a system of sparks that drift about the center as a set of concentric “rings”. Assuming that the spark width and separation are both equal to the gap height, they define a

nal itself. The observed modulation index (for which they reported 1.032 ± 0.001 and 1.034 ± 0.003 in the main pulse and interpulse respectively) is then given by $(1 + 2m^2)^{1/2}$. In the use of integrated samples this additional variance is reduced by the reciprocal of the time-bandwidth product and is typically neglected.

“complexity parameter” (a), equal to the ratio of spark width to the width of the polar cap, which they calculate as

$$a = 5 \left(\frac{\dot{P}}{10^{-15}} \right)^{2/7} \left(\frac{P}{1 \text{ s}} \right)^{-9/14}, \quad (12)$$

where P is the pulsar spin period. Since the space between sparks is equal to their width, the total number of sparks across the cap is $\sim a$, and the number of nested cones of emission (excluding the centre spark) is $n \approx (a - 1)/2$. They show that the complexity parameter is correlated with profile morphology, with core single profiles having the highest complexity parameters, followed by triple profiles and then multiple and conal single profiles. This leads them to suggest that core single profiles, and the central components of triple profiles, are the result of emission from a large number of narrow cones, broadened by the finite beam-width of the elementary emission ($2/\gamma$, where γ is the Lorentz factor of the emitting particles). This explains why their profile morphology is simple, and makes the prediction that the modulation index of such pulsars should be small.

In Figure 17 we plot lines of constant complexity parameter along with the period and intrinsic period derivative for 46 field pulsars presumed to be recycled ($P < 0.1 \text{ s}$, $\dot{P} < 10^{-15}$). We used the published proper motions of Toscano et al. (1999) and Lange et al. (2001), plus a new measurement for PSR J1518+4904 ($\mu = 7.5 \pm 0.7 \text{ mas yr}^{-1}$; Stappers unpublished), in combination with the Galactic potential model of Kuijken & Gilmore (1989) to correct the observed period derivatives for the effects of acceleration with respect to the line of sight (Damour & Taylor 1991). These points are shown as solid circles, while uncorrected points are not filled. The sources for which the modulation properties are now known are labelled. For most sources the model predicts 1–3 cones of emission, implying complex profiles with significant modulation, as observed. The exception to this statement is PSR B1937+21, with a large complexity parameter of $a \approx 23$. This pulsar is also exceptional for its low modulation index and simple profile morphology, just as expected for a large number of unresolved cones. We have already drawn an analogy between PSR B1937+21 and PSR B2053+36, and it is interesting to note that the complexity parameter of the latter is also quite high: $a \approx 10$. Indeed, Weisberg et al. (1986) found that not only PSR B2053+36, but all of the core-dominated pulsars in their sample have low modulation indices, in excellent agreement with the assertion, made by Gil & Sendyk (2000) on the basis of the tendency for core pulsars to have large complexity parameters, that core components are the sum of numerous $1/\gamma$ -smeared components.

We have shown that the detection and characterization of pulse-to-pulse intensity fluctuations in millisecond pulsars is possible using existing instruments. The acquisition of similar information about southern recycled pulsars and those accessible from Arecibo should expand the available sample and make stronger generalizations about the population possible. With the possible future availability of very large radio telescopes such as LOFAR and SKA both the number of recycled pulsars within the reach of study, and the depth of detail to which they

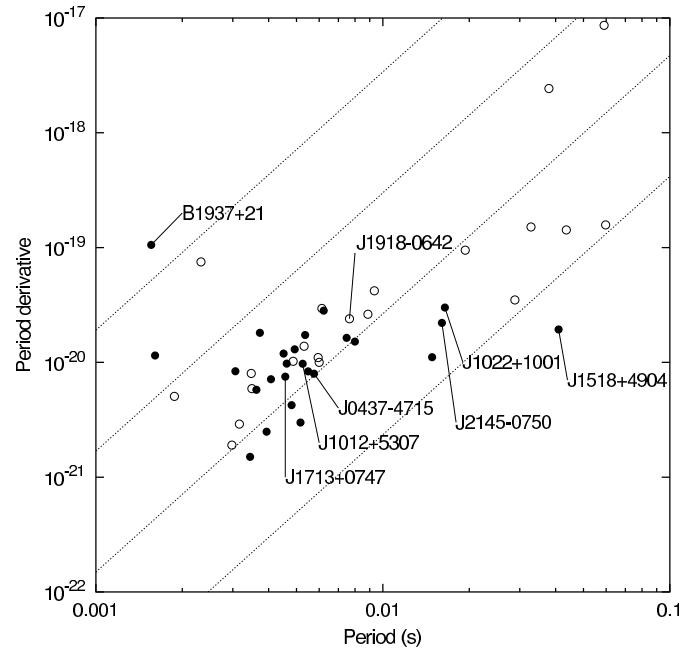


Fig. 17. Period vs Period derivative for 46 recycled pulsars in the Galactic disk. The solid points have been corrected for acceleration effects, the unfilled points have not. The dotted lines correspond to lines of equal value in the complexity parameter of Gil & Sendyk (2000), $a = 20, 10, 5, 2.5$ (top to bottom).

could be studied will be greatly enhanced and hopefully provide considerable constraining information on recycled pulsar polar caps and magnetospheres.

Acknowledgements. We thank R. Strom, A. Lommen, R. Ramachandran and M. Kramer for allowing us to use data originally recorded for other projects. RTE is supported by a NOVA fellowship. The WSRT is operated by ASTRON with financial support from the Netherlands Organisation for Scientific Research (NWO).

References

- Backer, D. C. 1970, *Nature*, 227, 692
- 1973, *ApJ*, 182, 245
- 1995, *J. Astrophys. Astr.*, 16, 165
- Backer, D. C., Kulkarni, S. R., Heiles, C., Davis, M. M., & Goss, W. M. 1982, *Nature*, 300, 615
- Backer, D. C., Rankin, J. M., & Campbell, D. B. 1975, *ApJ*, 197, 481
- Bartel, N., Sieber, W., & Wolszczan, A. 1980, *A&A*, 90, 58
- Cognard, I., Shrauner, J. A., Taylor, J. H., & Thorsett, S. E. 1996, *ApJ*, 457, L81
- Damour, T. & Taylor, J. H. 1991, *ApJ*, 366, 501
- Deshpande, A. A. & Rankin, J. M. 2001, *MNRAS*, 322, 438
- Edwards, R. T. & Stappers, B. W. 2002, *A&A*, 393, 733
- Edwards, R. T., Stappers, B. W., & van Leeuwen, A. G. J. 2003, *A&A*, 402, 321
- Foster, R. S., Fairhead, L., & Backer, D. C. 1991, *ApJ*, 378, 687
- Gil, J. & Krawczyk, A. 1997, *MNRAS*, 285, 561
- Gil, J. A. & Sendyk, M. 2000, *ApJ*, 541, 351
- Hankins, T. H., Kern, J. S., Weatherall, J. C., & Eilek, J. A. 2003, *Nature*, 422, 141

- Jenet, F., Anderson, S., Kaspi, V., Prince, T., & Unwin, S. 1998, *ApJ*, 498, 365
- Jenet, F. A., Anderson, S. B., & Prince, T. A. 2001, *ApJ*, 546, 394
- Karastergiou, A., von Hoensbroech, A., Kramer, M., et al. 2001, *A&A*, 379, 270
- Kinkhabwala, A. & Thorsett, S. E. 2000, *ApJ*, 535, 365
- Kramer, M. & Xilouris, K. M. 2000, in *Pulsar Astronomy - 2000 and Beyond*, IAU Colloquium 177, ed. M. Kramer, N. Wex, & R. Wielebinski (San Francisco: Astronomical Society of the Pacific), 229–234
- Kuijken, K. & Gilmore, G. 1989, *MNRAS*, 239, 571
- Lange, C., Camilo, F., Wex, N., et al. 2001, *MNRAS*, 326, 274
- Phinney, E. S. & Kulkarni, S. R. 1994, *Ann. Rev. Astr. Ap.*, 32, 591
- Popov, M. V. 1986, *Sov. Astron.*, 30, 577
- Popov, M. V. & Stappers, B. W. 2003, *Astronomy Reports*, in press.
- Rankin, J. M. 1986, *ApJ*, 301, 901
- Ritchings, R. T. 1976, *MNRAS*, 176, 249
- Romani, R. & Johnston, S. 2001, *ApJ*, 557, L93
- Ruderman, M. A. & Sutherland, P. G. 1975, *ApJ*, 196, 51
- Sallmen, S. 1998, PhD thesis, University of California at Berkeley
- Sallmen, S. & Backer, D. C. 1995, in *Millisecond Pulsars: A Decade of Surprise*, ed. A. S. Fruchter, M. Tavani, & D. C. Backer (*Astron. Soc. Pac. Conf. Ser. Vol. 72*), 340–342
- Taylor, J. H. & Huguenin, G. R. 1971, *ApJ*, 167, 273
- Taylor, J. H., Manchester, R. N., & Huguenin, G. R. 1975, *ApJ*, 195, 513
- Toscano, M., Sandhu, J. S., Bailes, M., et al. 1999, *MNRAS*, 307, 925
- Vivekanand, M. 2002, *MNRAS*, 332, 55
- Vivekanand, M., Ables, J., & McConnell, D. 1998, *ApJ*, 501, 823
- Voûte, J. L. L., Kouwenhoven, M. L. A., van Haren, P. C., et al. 2002, *A&A*, 385, 733
- Weisberg, J. M., Armstrong, B. K., Backus, P. R., et al. 1986, *AJ*, 92, 621
- Weisberg, J. M. & Taylor, J. H. 2002, *ApJ*, 576, 942
- Wolszczan, A., Cordes, J. M., & Stinebring, D. R. 1984, in *Millisecond Pulsars*, ed. S. P. Reynolds & D. R. Stinebring (Green Bank: NRAO), 63–70